

Project no.:  
**229196**

Project acronym:  
**piezoVolume**

Project full title:  
*High volume piezoelectric thin film production process for microsystems*

**Collaborative Project targeted to a special group (such as SMEs)**  
**Grant Agreement No.:**

**NMP2-SE-2009-229196**

Start date of project: 2010-01-01  
Duration: 3 years

**D 4.5**  
**Final report for testing of device prototypes for  
performance, reliability and lifetime**

Due delivery date: 2012-11-30  
**Actual delivery date: 2012-12-21**

Organisation name of lead contractor for this deliverable: OCE

Project co-funded by the European Commission within the Seventh Framework Programme (2008-2011)		
Dissemination Level		
<b>PU</b>	Public	X
<b>PP</b>	Restricted to other programme participants (including the Commission Services)	
<b>RE</b>	Restricted to a group specified by the consortium (including the Commission Services)	
<b>CO</b>	Confidential , only for members of the consortium (including the Commission Services)	

<b>Deliverable number:</b>	D 4.5
<b>Deliverable name:</b>	Final report for testing of device prototypes for performance, reliability and lifetime
<b>Work package:</b>	WP 4 Testing and characterization
<b>Lead contractor:</b>	AIX

<b>Author(s)</b>		
<b>Name</b>	<b>Organisation</b>	<b>E-mail</b>
Wilfred Booij	Sonitor	Wilfred.Booijsonitor.com
Igor Shklyarevskiy	Océ	Igor.Shklyarevskiy@oce.com
Tonni Franke Johansen	SINTEF	Tonni.F.Johansen@sintef.no
Cyril Meynier	VERMON	c.meynier@vermon.com
An Nguyen-Dinh	VERMON	An.nguyendinh@vermon.com

<b>Abstract</b>
This document gives an overview and summary of the testing of piezoVolume devices during the project

<b>Public introduction<sup>1</sup></b>

---

<sup>1</sup> According to Deliverables list in Annex I, all restricted (RE) deliverables will contain an introduction that will be made public through the project WEBSITE

---

## TABLE OF CONTENTS

---

	Page
1	GENERAL PZT FILM PERFORMANCE (AIX) ..... 4
1.1	Homogeneity Check of the deposited material..... 4
1.2	Large and small signal properties of the film ..... 5
1.3	Reliability of film properties ..... 6
2	OCE INKJET ACTUATOR..... 8
2.1	Sample description ..... 8
2.2	Experimental methods ..... 9
2.3	Device evaluation ..... 11
2.3.1	Performance ..... 11
2.3.2	Reliability / Operation stability ..... 14
2.3.3	Life-time ..... 15
2.4	Performance vs. specifications ..... 16
2.5	Performance vs. competitive technologies ..... 16
2.6	Conclusions & dissemination plans..... 16
3	SONITOR MICROPHONE DEVICES ..... 17
3.1	Device properties ..... 17
3.1.1	Low imposed stress and fatigue..... 17
3.2	Important Microphone characteristics ..... 18
3.3	Low acoustic sensitivity and characterization challenges ..... 18
3.4	Industry baseline – ECM characterisation..... 18
3.4.1	ECM sensitivity in the ultrasonic frequency range (40-60 kHz)..... 18
3.4.2	ECM test methodology ..... 19
3.4.3	Sensitivity characterization of piezovolume devices..... 22
3.5	Replacing ECM with piezoMEMS based microphones ..... 22
3.6	Background..... 22
3.7	Impedance Measurement results ..... 23
3.8	Conclusions ..... 23
4	VERMON PMUT..... 24
4.1	Geometric control ..... 24
4.2	Identification of modes by impedance measurements in air ..... 26
4.2.1	Modes of a clamped circular membrane..... 26
4.2.2	Impedance measurement ..... 27
4.3	Laser interferometry measurements ..... 28
4.3.1	Principle ..... 28
4.3.2	Measurements in air..... 28
4.3.3	Measurements in oil..... 30
4.3.4	Wideband excitation ..... 30
4.3.5	Narrow band excitation at 750 kHz ..... 31
4.3.6	Conversion to acoustic intensity ..... 32
4.4	Conclusion ..... 33

---

## 1 GENERAL PZT FILM PERFORMANCE (AIX)

General film performance of the PZT gives feedback on properties and reliability right after top electrode structuring, before costly processing steps like back side etching are required. First of all large and small signal properties of the deposited material will be recorded. The wafer map allows to give feedback for process optimization of the deposition process and shows the homogeneity or in wafer variation of a certain property. After this general performance check, reliability of the film properties can be investigated.

### 1.1 Homogeneity Check of the deposited material

The DBLI tool build in Task 2.3 allows to acquire wafer mapping information. Green represents a quite homogenous distribution of properties.

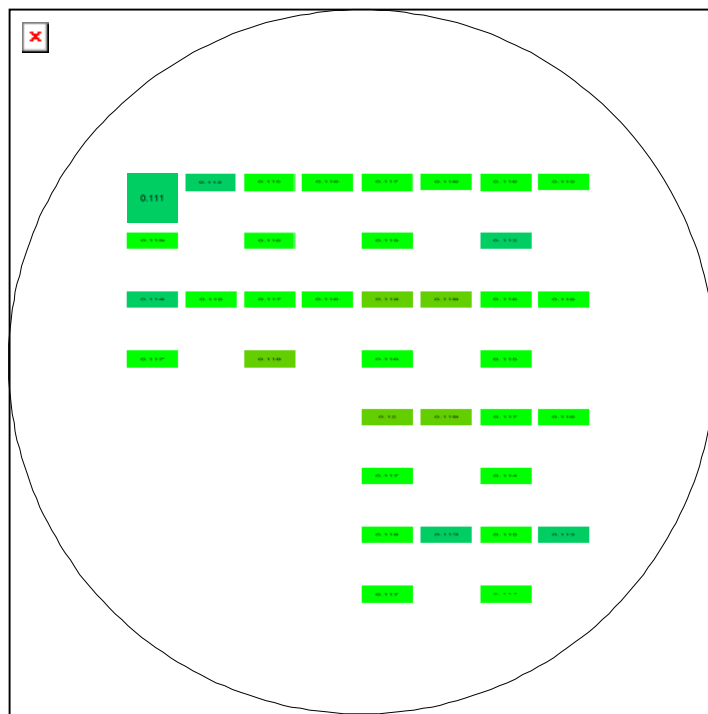


Figure 1.1: Wafer mapping information on pV053 showing nice homogeneity

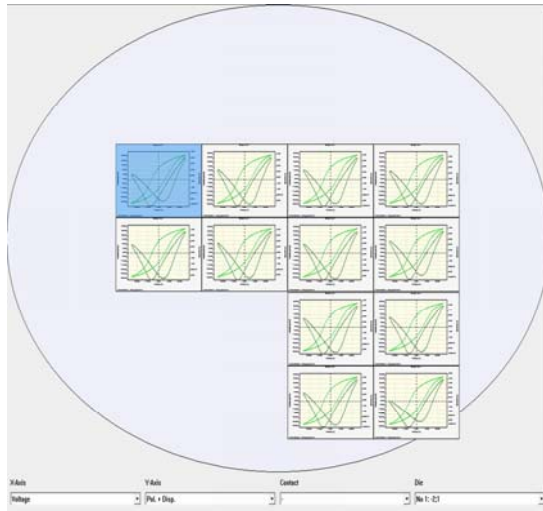


Figure 1.2: Wafer map with P-E and butterfly loop on pV 053

## 1.2 Large and small signal properties of the film

The basis measurements that have been performed on the films are small signal measurements of dielectric constant and piezoelectric coefficient and large signal measurements of displacement and polarization. Both results are shown in figure 1.3

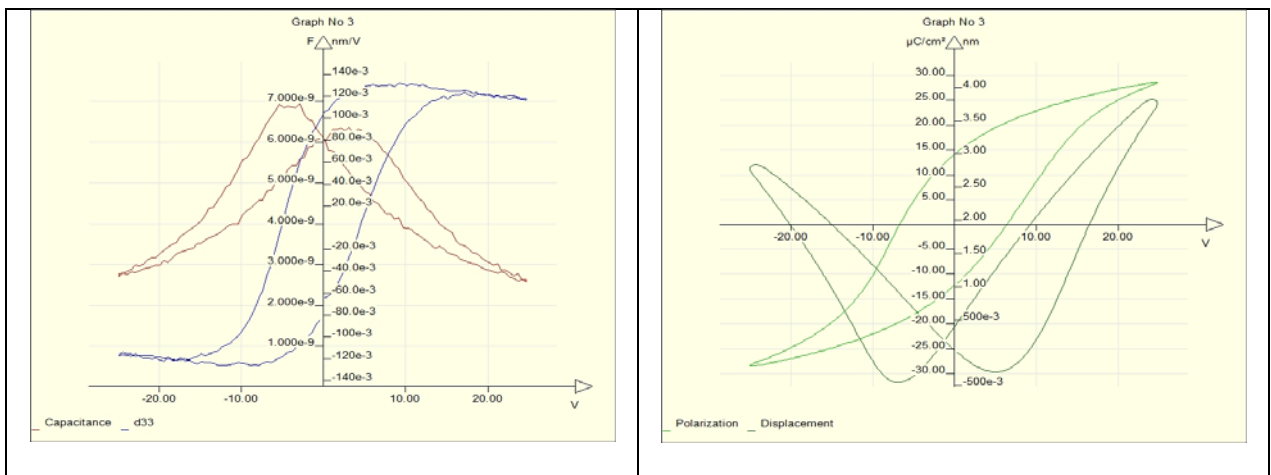


Figure 1.3 Small signal and large signal material properties of PZT thin films.

Beside these basic measurement, leakage current and piezoelectric coefficient  $e_{31,f}$  and breakdown voltage have been tested. The breakdown voltage of a  $4\mu\text{m}$  thick sol gel film is shown in figure 1.4



Figure 1.4: Breakdown test using voltage ramp of 1V/second, pad size

### 1.3 Reliability of film properties

Reliability tests of the piezoelectric film have been performed in terms of fatigue and DC creep. Figure 1.xxx shows the creep of the unipolar hysteresis after DC voltage treatment of 10000s. There is a non neglectable change of the behavior which would influence the operation of an actuator.

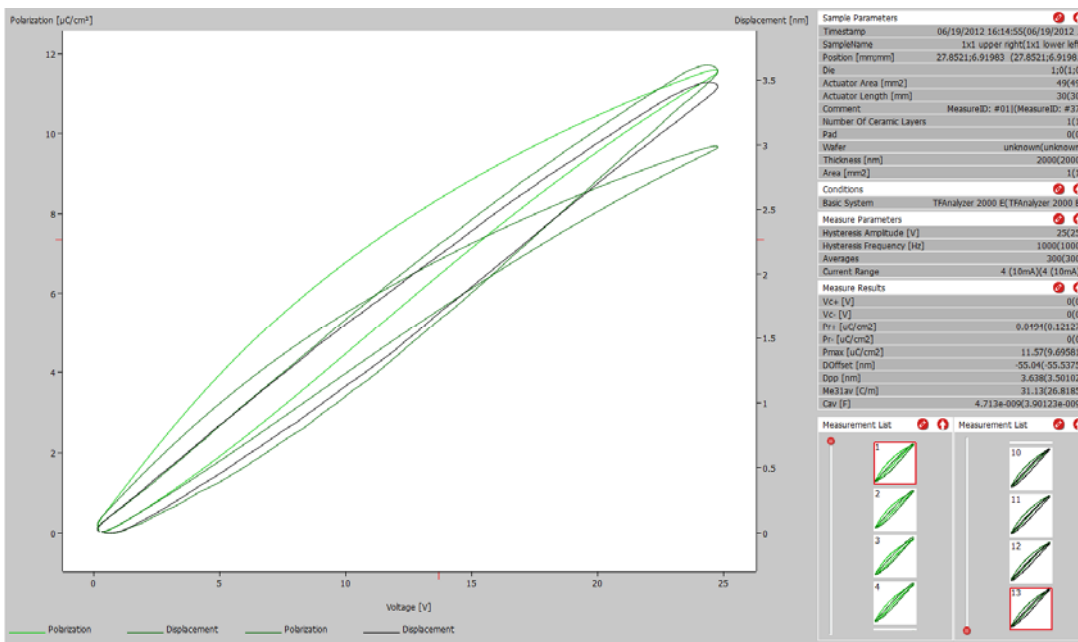


Figure: DC creep of sol gel deposited sample, showing stronging degradation behavior

The fatigue behavior of the sputtered films which shows no degradation for  $10^8$  cycles is very good as shown in figure 1.xxx

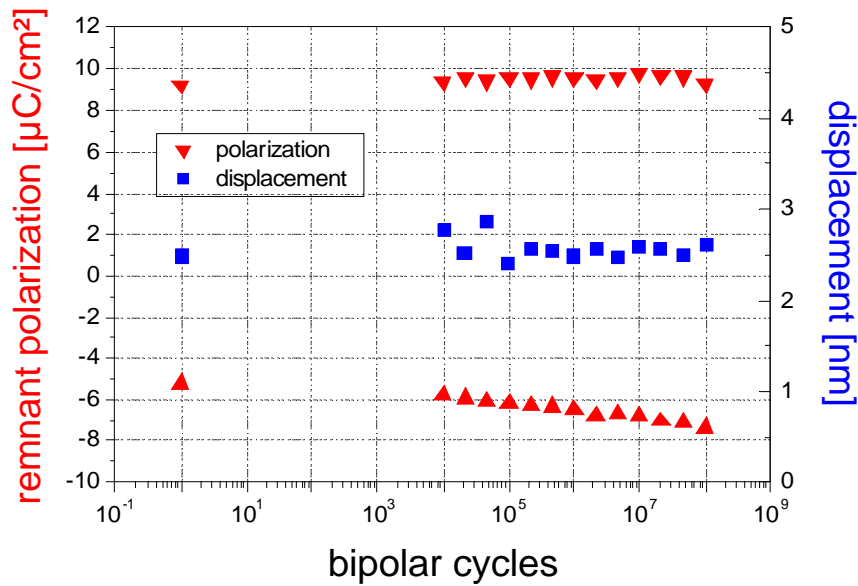


Figure1: Fatigue behavior at 1kHz and different voltages on sol gel deposited films

Investigating of the fatigue behavior at different voltages and different frequencies have been performed and do not show dependencies on the varied parameter up to  $10^7$  cycles.

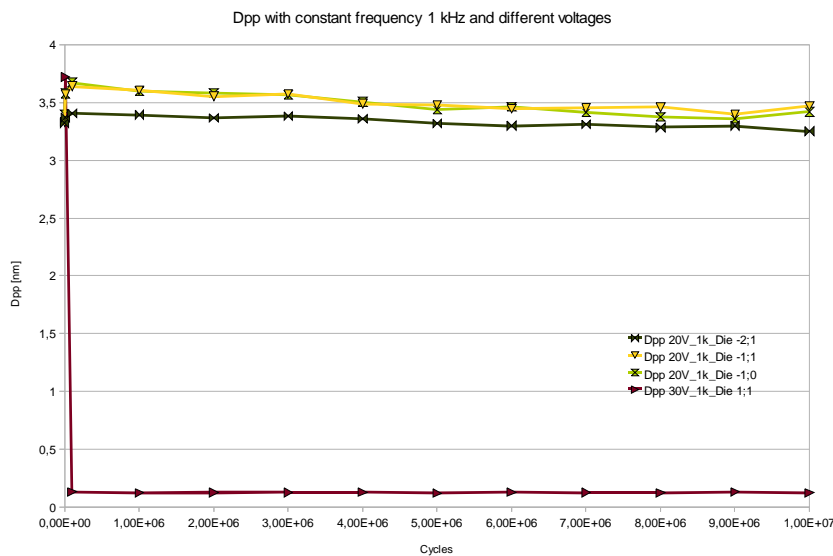


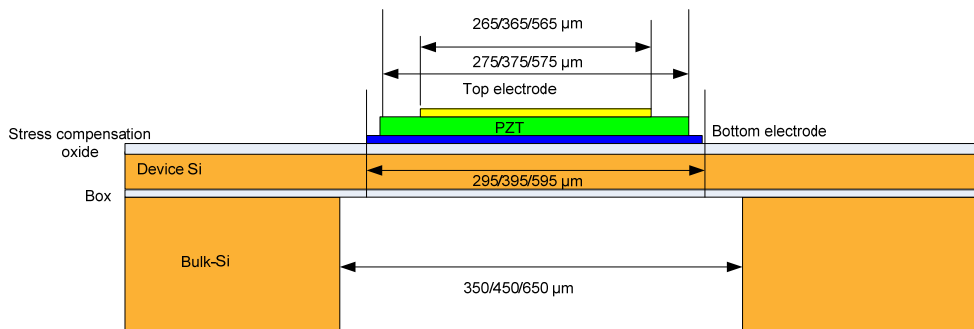
Figure2: Fatigue behavior of sol gel deposited films at 1kHz and different voltages

## 2 OCE INKJET ACTUATOR

### 2.1 Sample description

Several designs of inkjet actuators were realized as prototype devices in generation 1 and 2. The dimensions and photos are presented in Figure 1. There is no design difference between generation 1 and 2.

Cross section:



Top view:

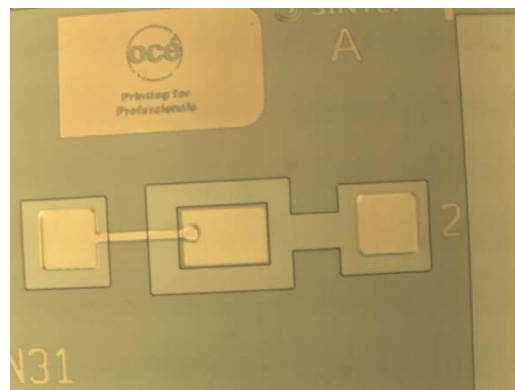
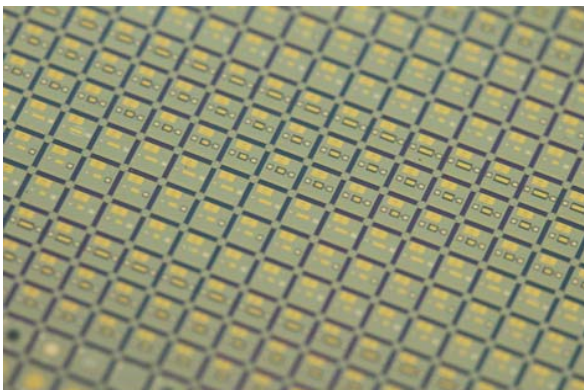
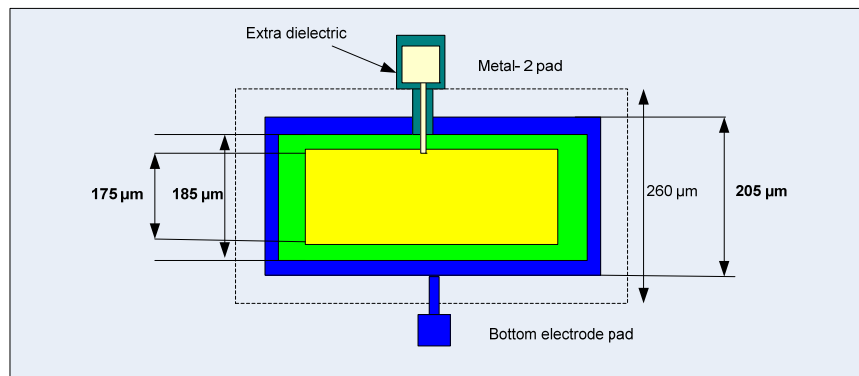


Figure 1. Top: cross section and top view of the ink jet actuator design. Bottom: photos of the realized prototypes.

## 2.2 Experimental methods

Out-of-plane deflection was measured using Polytec SLV with MSA-400 optical measurement head at 10 kHz (Figure 2) using two driving methods described below. Additionally this setup was used for evaluation of the device stability/reliability.

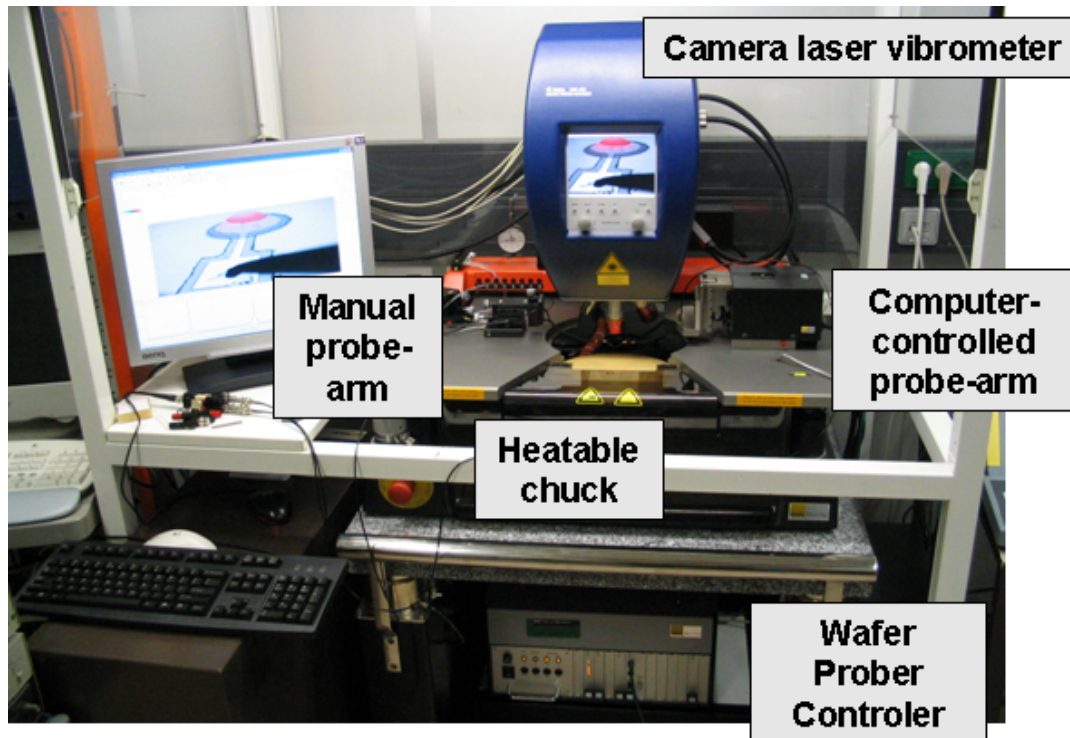


Figure 2. Photo of the measurement setup

### *Bias sweep + small ac ripple (method #1)*

Figure 3 shows schematically the principle of the driving method #1 and corresponding test device behaviour. In this method, *dc* bias sweep was performed with a small overlapping *ac* ripple (1 V). The device response can be described as following: application of the *dc* component results in the device static deflection. Application of the small *ac* ripple, in its turn, results in the small vibrations of the device at given frequency around the static deflection value reached due to bias application. Variation of the *dc* voltage allows measuring the deflection amplitude as a function of bias (Bias varied in the range  $0V \rightarrow 30V \rightarrow 0V \rightarrow -30V \rightarrow 0V \rightarrow 30V \rightarrow 0V$ ). Thus driven PZT layer will exhibit only intrinsic contributions to the piezoelectric effect.

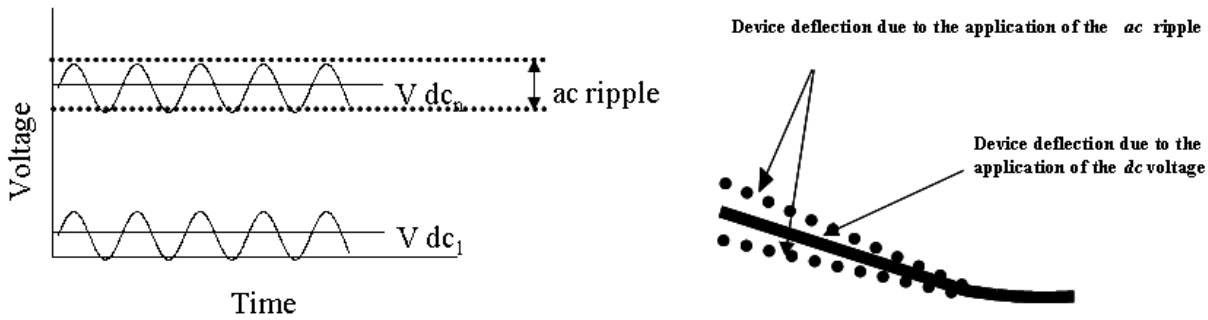


Figure 3. Schematic representation of the first driving method (left), and corresponding test device behavior (right)

**Large ac amplitude + equal dc bias (method #2)**

Figure 4 shows schematically the principle of the driving method #2 and corresponding device behaviour. The experimental procedure can be described as following: application of the *dc* component results in the device static deflection. Application of the *ac* component, in its turn, results in the device vibration at given frequency. By measuring the deflection at  $V_{ac} = V_{dc}$  we acquire a total deflection at given voltage. Variation of the *dc* voltage allows measuring the deflection as a function of voltage (Bias and *ac* varied in the range  $0V \rightarrow 15V \rightarrow 0V \rightarrow -15V \rightarrow 0V$ ). This driving method excites both intrinsic and extrinsic contributions to the piezoelectric effect.

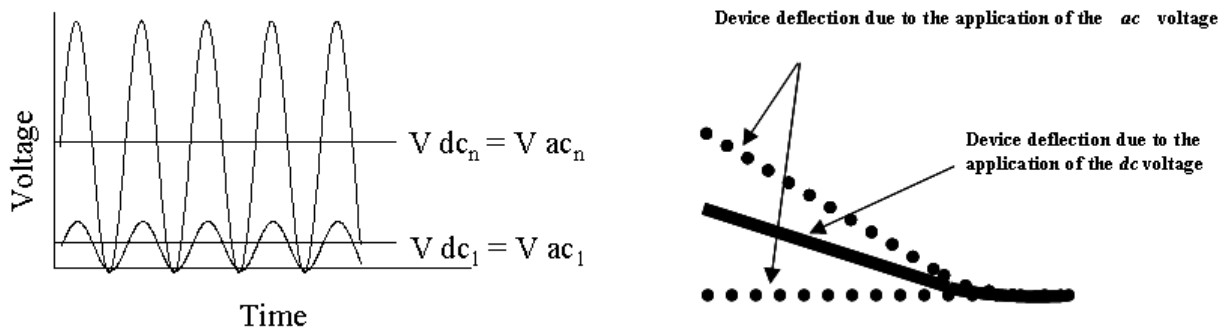


Figure 4. Schematic representation of the second driving method (left) and corresponding test device behavior (right)

Both methods provide an access to the butterfly loops associated with the ferroelectric switching as shown in Figure 5. The left panel demonstrates the part of the butterfly curve probed by method #1 and the right panel – probed by method #2. We can also see that, effectively, method #1 measures a differential of the method #2. In reality it is not the truth due to different piezoelectric contributions stimulated by these two driving methods.

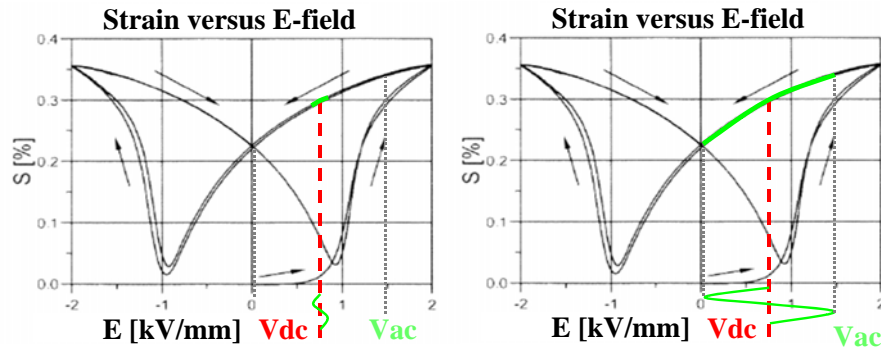


Figure 5. The parts of the butterfly loops probed by two driving methods (left - method #1, right - method #2)

## 2.3 Device evaluation

### 2.3.1 Performance

#### Generation 1

#### Wafer PV209

Figure 6 shows butterfly loops consequently measured on device from PV209 wafers by driving method #1. The devices under investigation were not poled in advance. The measurement temperature was 25°C. To our surprise, consequent bias cycling sweep resulted in substantial deflection reduction in positive voltage region. Such behavior was never observed before, so we find it difficult to interpret these results.

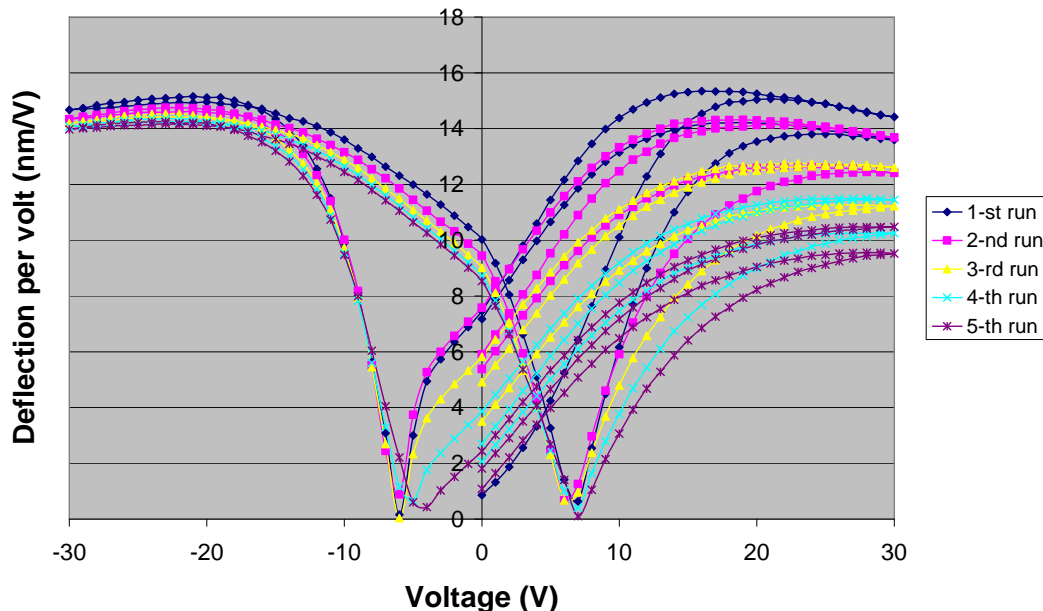


Figure 6. Butterfly loops consequently measured on device from PV209 wafers by driving method #1. The deflection decrease at positive bias values is not understood yet.

Figure 7 shows butterfly loops consequently measured on device from PV209 wafers by driving method #2. Measurements conditions remain the same as in the previous experiment. It can be clearly seen that the large signal butterfly loops are strongly asymmetrical. This might be due to imprint or self-polarization of the PZT film occurred during deposition process. In fact in our

case this effect is highly welcome as it should result in stable deflection of the membrane as well as rendering poling procedure unnecessary. To check the above we have performed stability experiments on this wafer.

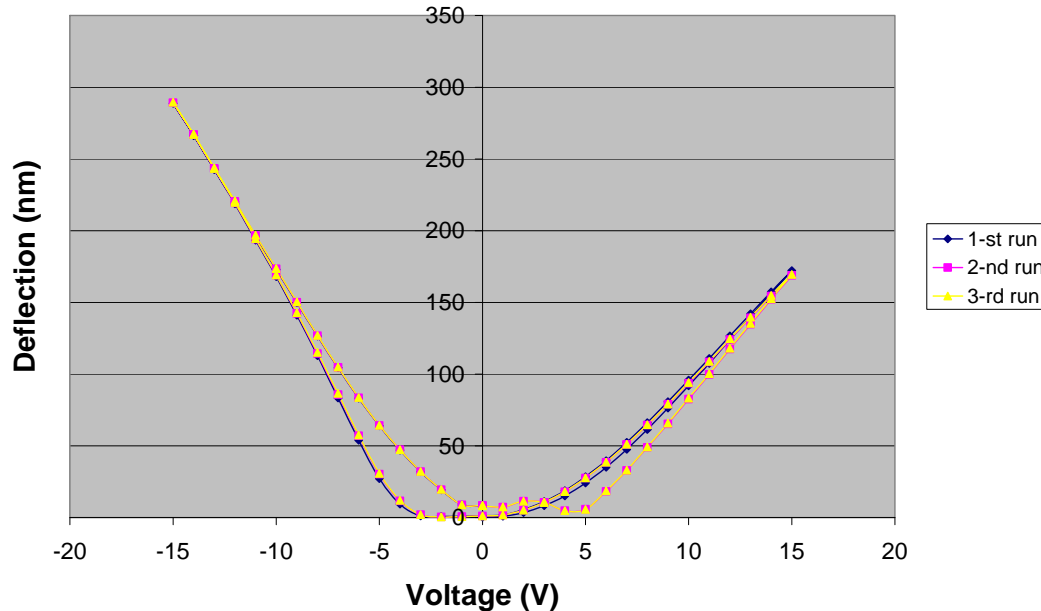


Figure 7. Butterfly loops consequently measured on device from PV209 wafers by driving method #2.

### Wafer PV201

The device deflection measured on the chips from wafer PV201 in two regimes is presented on Figure 8 and Figure 9. Clearly, the deflection of these devices is lower than that of those from PV209. Yet it is not clear if it is related to PZT material properties, or, possibly, membrane thickness variation. Another difference between these two wafers is that butterfly loops measured on PV201 are symmetrical and do not decrease after subsequent runs.

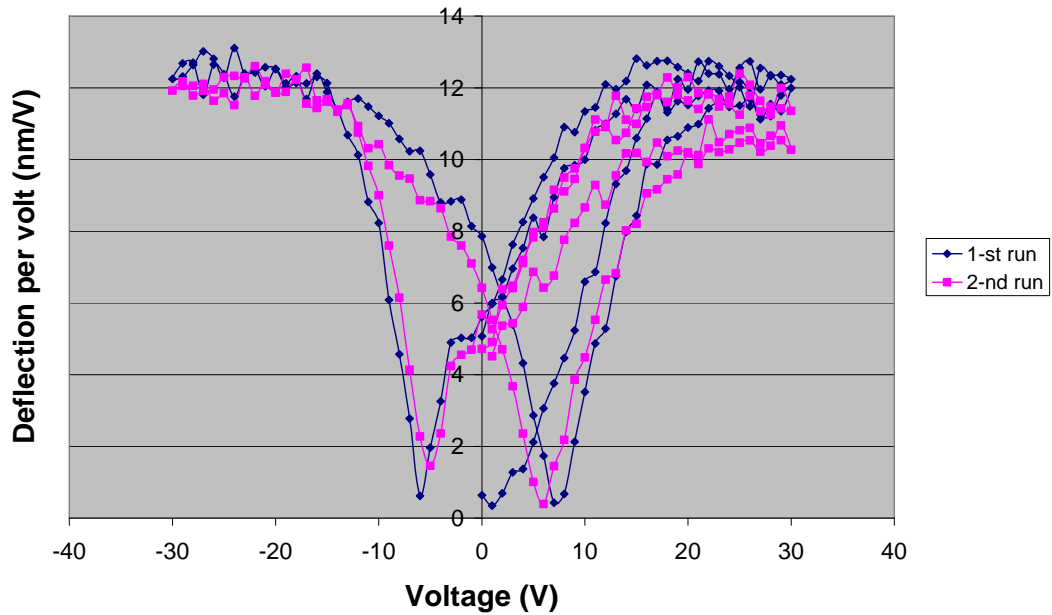


Figure 8. Butterfly loops consequently measured on device from PV201 wafers by driving method #1.

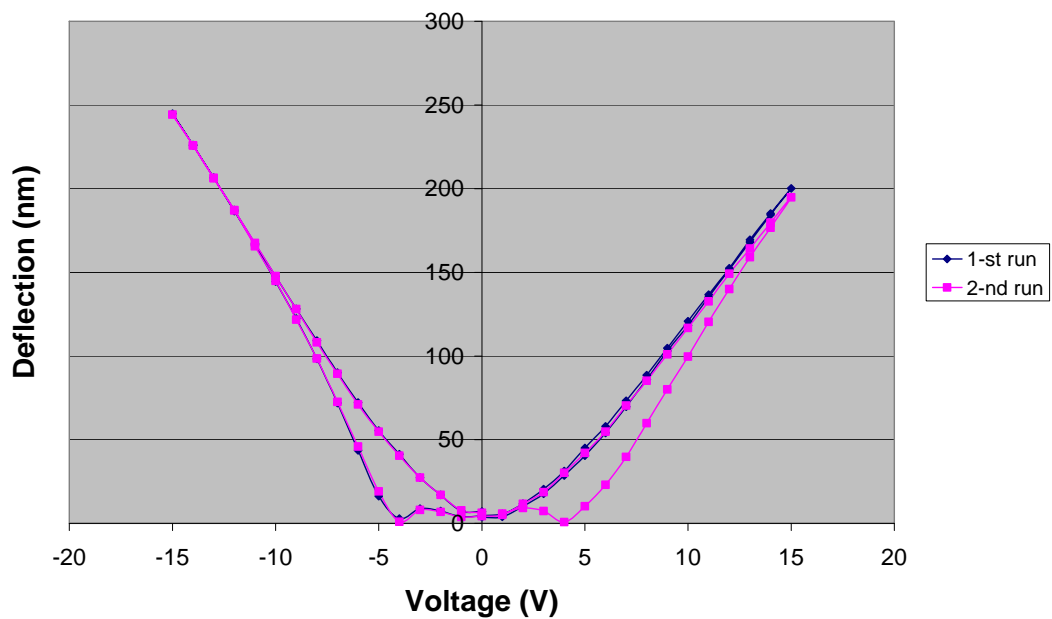


Figure 9. Butterfly loops consequently measured on device from PV201 wafers by driving method #2.

## Generation 2

### **Wafer PV202**

The results obtained on generation 2 devices are shown in Figure 10 and Figure 11 below. The major improvement as compared to the Gen 1 is slightly higher breakdown voltage ( $\sim 20$  V/ $\mu\text{m}$ ).

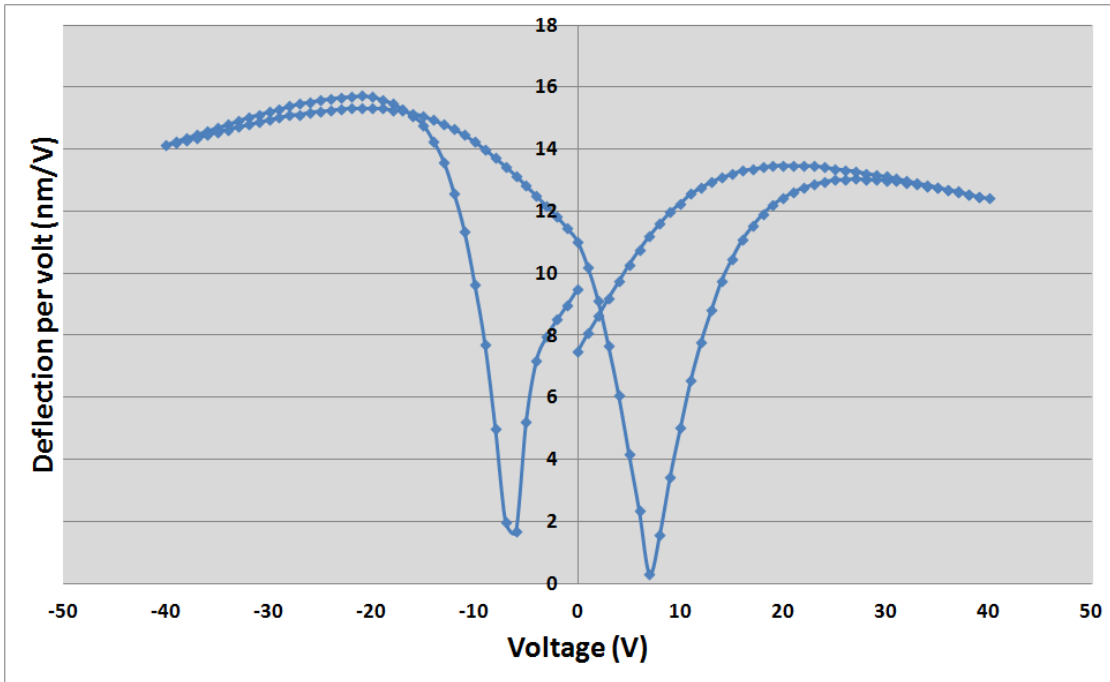


Figure 10. Butterfly loops consequently measured on device from PV202 wafers by driving method #1.

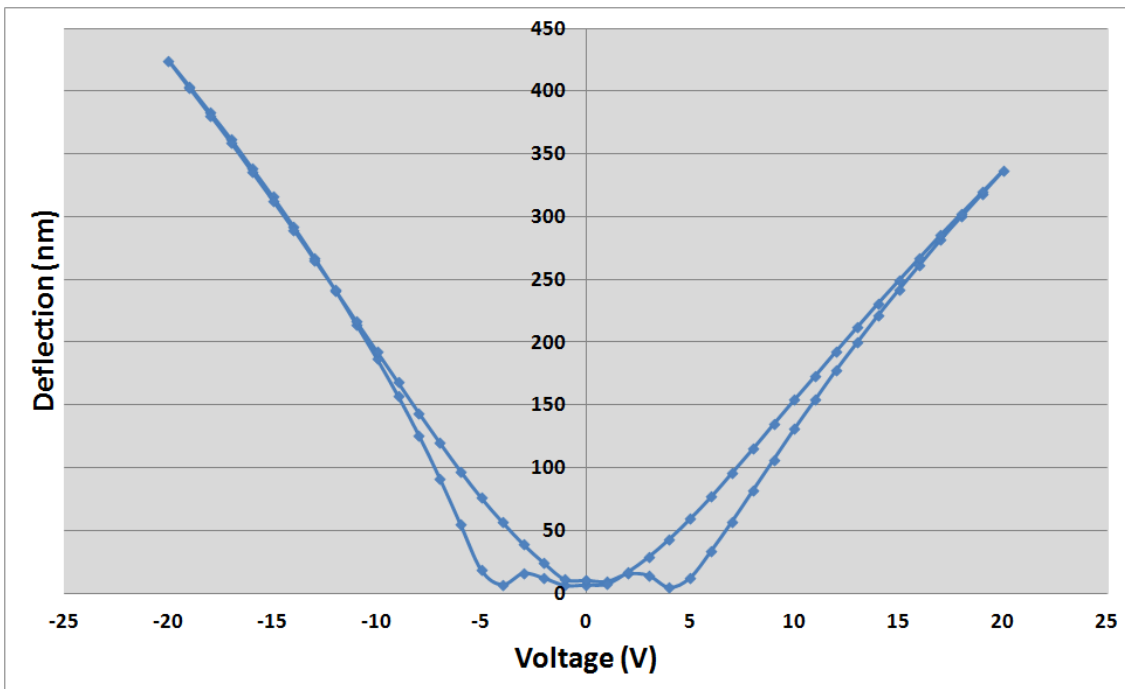


Figure 11. Butterfly loops consequently measured on device from PV202 wafers by driving method #2.

### 2.3.2 Reliability / Operation stability

Stability experiments were performed by driving the actuator device in large signal regime (close to the real life application regime) at  $\pm 15\text{Vdc} + 15\text{Vac}$  @ 100KHz. Figure 12 shows the results of the stability experiment. To visualize the membrane stability we plotted normalized deflection on the y-axis. The deflection is normalized on the first measured value. It can be seen

that at negative bias (-15Vdc + 15Vac dark blue line) the initial deflection increases by 60% and eventually stabilizes at about 140% of the initial value. This represents a quite acceptable situation for our device, which, in the real life, might require slight preconditioning of PZT layer.

However, the stability measurements performed with the opposite bias polarity show completely different picture (Figure 12 light blue line). Actuator deflection under +15Vdc + 15Vac driving conditions, though slightly increasing in the beginning, shows strong decrease after 15 minutes of actuation, which decreases to virtually zero after 30 minutes.

In the meantime the requirements for high temperature operation (130 °C) became obsolete. Therefore the operation stability experiments were performed at ambient temperatures. Based on the obtained results, we can say that the performance of the devices is satisfactory under negative bias and unacceptable under opposite one.

Yet, the attention point of quite low breakdown voltage (15-25 V/um) remains!

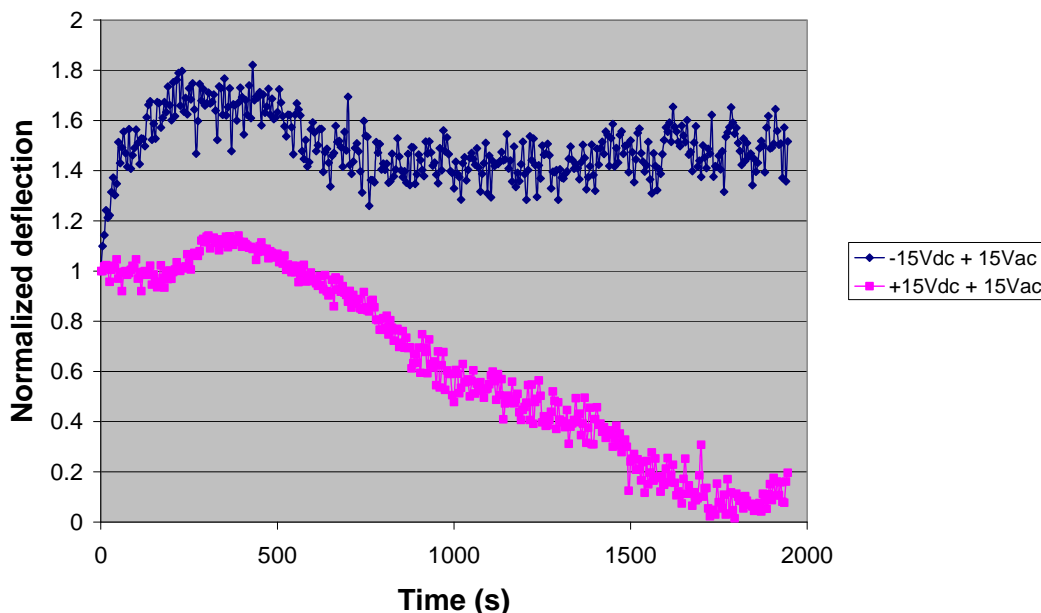


Figure 12. Normalized actuator deflection measured at -15Vdc +15Vac (dark blue line) and 15Vdc +15Vac (light blue line) @ 100KHz, ambient.

### 2.3.3 Life-time

Devices from Gen 1 and Gen 2 were tested on electrical breakdown. No difference between wafers or processing methods (routed-off top electrode vs standard processing) was found. The breakdown voltage for Gen 1 devices was measured to be slightly above 30V and from Gen 2 – slightly above 40V, which lower than expected and, possibly, needed for our application.

Unfortunately, due to low breakdown voltage reported above no reliable HALT (Highly Accelerated Life-Time) experiments could be performed. It is a point of attention for future generation devices.

## 2.4 Performance vs. specifications

Device performance in both cases represents a satisfactory case. The deflection values are sufficient for the realization of the necessary volume displacement for droplet ejection. Unfortunately, we were not able to implement the PV layers in the real demonstrator due to unavailability of wafers with PZT.

## 2.5 Performance vs. competitive technologies

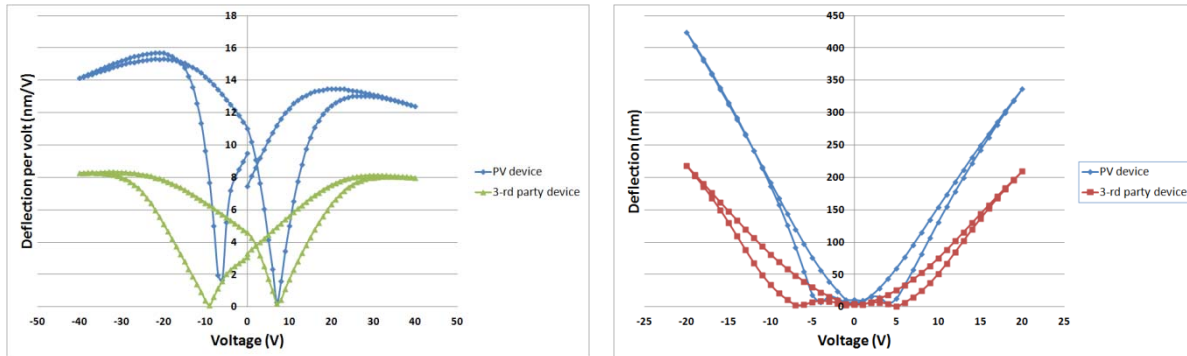


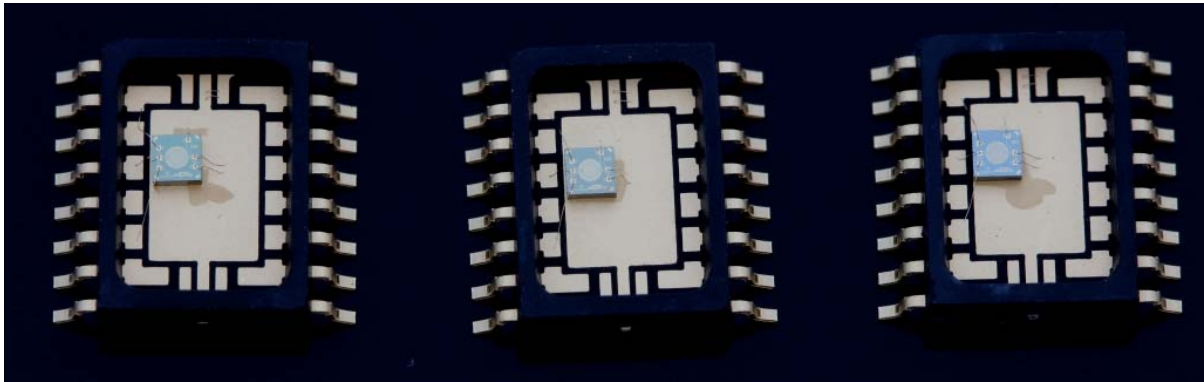
Figure 13. Comparison of the deflection measured on the identical devices with PV PZT layer and the PZT layer deposited by the third party.

Figure 13 above shows the small signal deflection with ac ripple of 1V (left), and large signal deflection with ac=dc (right). Blue lines represent the deflection measured on PiezoVolume devices while the red one corresponds to the deflection of the identical device but with the PZT layer from the third party. Clearly, PZT material developed with PiezoVolume project is twice more efficient than the material used in the previous experiments at Océ.

## 2.6 Conclusions & dissemination plans

There are already several projects at Océ that are planning to utilize thin PZT layers as an active material for inkjet actuator. Despite several technical issues and the current absence of industrial source of “graded” PZT layers we believe that PiezoMEMS is the future technology for inkjet printing.

### 3 SONITOR MICROPHONE DEVICES



*Figure 14 microphone chips glued on SOIC packet, and bonded for connection to the packet's pins.*

#### 3.1 Device properties

Since the Sonitor devices are intended to be used as microphone devices, evaluation of the devices reliability and lifetime are challenging due to the following characteristics:

- The devices designed impose extremely low stress on the piezo-electric material due to the poor acoustic matching
- The devices have very low acoustic sensitivity and are very difficult to characterize in a repeatable fashion.

The consequence of these characteristics for lifetime and reliability measurements are expanded on.

##### 3.1.1 Low imposed stress and fatigue

Piezo-electric materials as used in this project have been shown to suffer fatigue type behavior when exposed to strains or excitation voltages of the saturation voltage of the films, which is of the order of 20 V. However, when used as microphonic sensing devices, the film is operated in entirely different regime. The best illustration of this is the fact that when the piezo-electric devices are driven by the highest pressure sound excitation achievable in our custom built equipment, the resulting sensed voltage is close to a million times below the saturation voltage:

**Sound pressure SPL** 103dB(rms) where 0dB = 20uPa(rms) = 2.825Pa

**Resulting Piezo mic sensed voltage:** -82dBV = 79uV(rms) (compare to 20V)

Based on these fundamental differences, fatigue as a source of reliability issue can therefore be in these devices. This was confirmed in a number of tests of microphone sensitivity over time which showed no significant changes beyond the noise in the measurement.

### 3.2 Important Microphone characteristics

One of the most important characteristic of a microphone is its sensitivity over the intended frequency use range. The ability to manufacture microphone elements within a specified sensitivity range (bin) over a certain frequency range is a key success factor for any commercial microphone manufacturer. As part of this project we therefore focused our attention on the ability to characterise microphone sensitivity over frequency in the ultrasonic range.

### 3.3 Low acoustic sensitivity and characterization challenges

It has been clearly shown through device characterization that the multiple project wafer restriction that is central in this project, imposes fundamental restrictions on the acoustical sensitivity that can be realized (see D3.2). The sensitivity of the best devices is of the order of -90 dB, this is a factor 1000 less than the best electret based microphones. As part of the project we have developed a setup based on the most common electret condenser module (ECM) characterization methodology encountered in the industry.

### 3.4 Industry baseline – ECM characterisation

The ECM is still the most commonly encountered microphone solution in today’s audio products. It combines high sensitivity, compactness and low cost that is still proving to be difficult to beat with MEMS based solutions. Sonitor has found that a fraction of commercially available audio ECM’s also show good sensitivity in the ultrasonic range of interest (40-60 kHz). A schematic showing the most commonly encountered ECM construction is shown below.

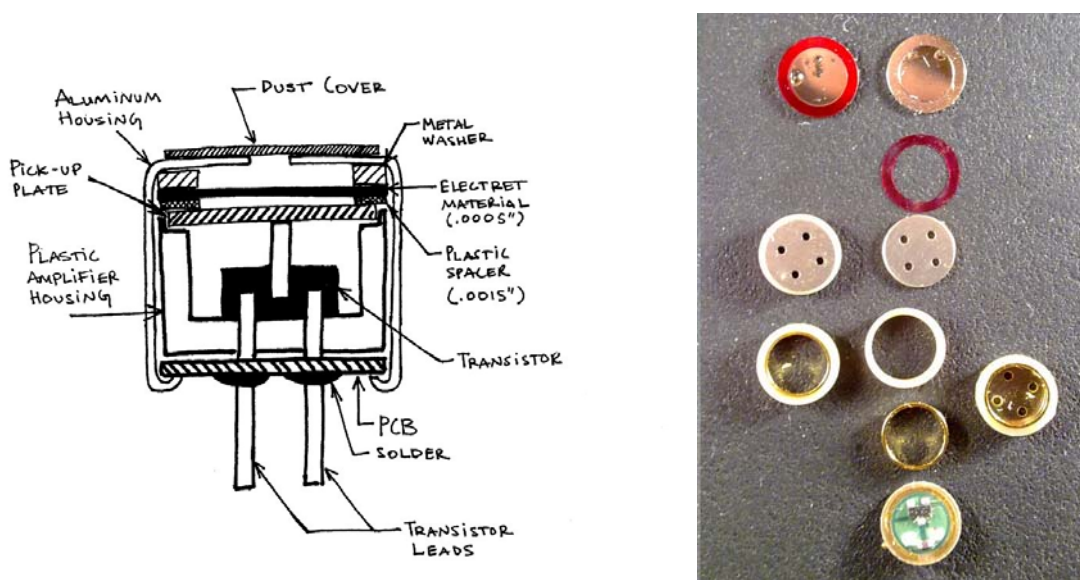


Figure 15 Typical construction used in a Back electret ECM, the industry workhorse. To the right the individual components used are shown.

#### 3.4.1 ECM sensitivity in the ultrasonic frequency range (40-60 kHz)

ECM sensitivity in the ultrasonic frequency range can be viewed as accidental rather than intentional. Typical high end audio application such as audio recording require no sensitivity of the microphone element beyond 20 kHz, the commonly accepted upper limit of human hearing. However, due to increasing pressure on miniturisation, the typical size of an ECM has shown a strong downward trend. Whereas 20 years ago, 10 mm diameter ECM components were common place, today's products deploy elements down to 4 mm in diameter. A fortunate consequence of this is, that as the size of the membrane shrinks, the natural resonance frequency of the microphone goes up. We therefore typically encounter good ultrasonic sensitivity on the smallest size ECM's. A typical example of a ECM with good ultrasonic performance up to 40 kHz is shown below. Typically such ECM's have a sensitivity of -40 to -30 dBm in the 40 kHz range. In comparison we find that the best piezovolume microphones have a sensitivity of -80 dB.

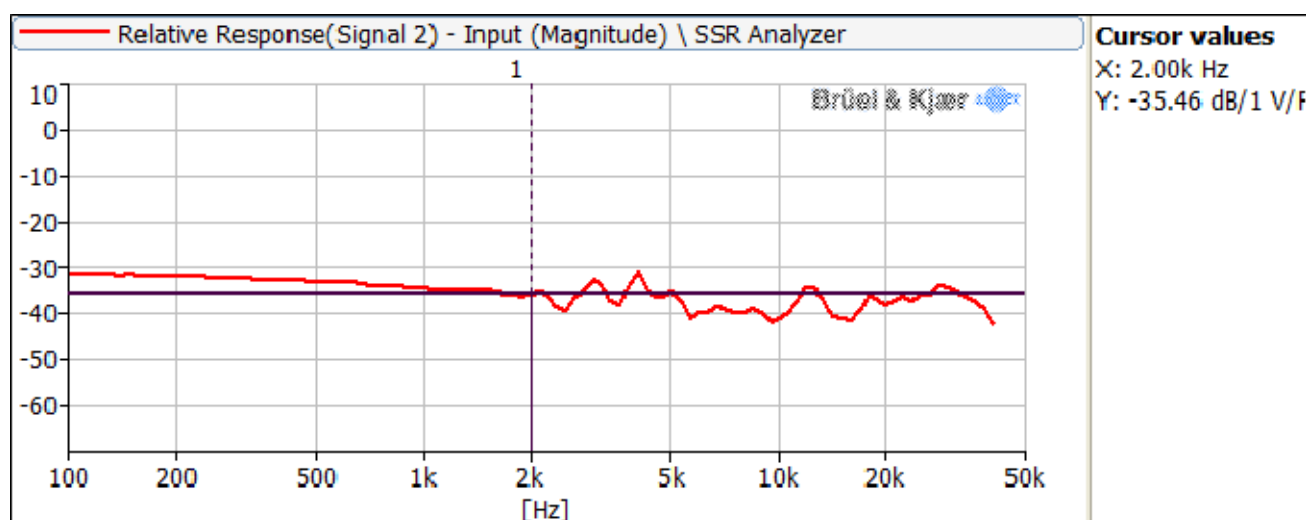


Figure 16 Typical frequency response of a low cost commercial ECM used in mobile phones

### 3.4.2 ECM test methodology

The ECM test methodology in industry is little known in normal scientific or even engineering literature. The ability to characterize microphone accurately in the least amount of time provides a competitive advantage and is therefore highly guarded as proprietary information. As part of a dissemination activity in this project we were fortunate to be able to visit one of our ECM suppliers. This Taiwanese supplier delivers up to 100K ECM modules a day to leading mobile phone vendors. The supplier is well versed in audio characterization of the ECM's they supply and had a highly optimized setup for high throughput testing of ECM's in the audio range. However, although they are the staple supplier for Sonitor product, the setup was inadequate in the ultrasonic range. This proved itself to be an excellent learning opportunity for this project. The vendor was willing to share their audio testing methodology in return for Sonitor extending the capability to the ultrasonic range.

The test methodology was simple but highly effective, resulting in a measurement interval of 5s per ECM. The principles deployed are as follows:

1. A highly stable and repeatable electro-acoustic transducer is used to create a high level acoustic excitation in the form of a broadband chirp (typically SPL 80 dB).
  - a. Typically an electret speaker as encountered in high end headphones is used

- b. By deploying a high end DAC with built-in calibration facilities as the electrical source, variability in the electrical stimulus is reduced to an absolute minimum.
2. The transducer is mounted in an anechoic box with multiple sound traps consisting of soft multi-layered cloth
3. The electret microphone is mounted upside down in a metallic receptacle that acts simultaneously as the electrical ground
4. A high end measurement microphone (e.g. B&K 3940) is used to measure the resulting excitation pulse at the exact location of the ECM and recorded as a calibration sensitivity trace.
5. The resulting electrical signal from the DUT is recorded using a ADC with built-in calibration capability.
6. The resulting measured signal is compensated for the measured calibration trace.

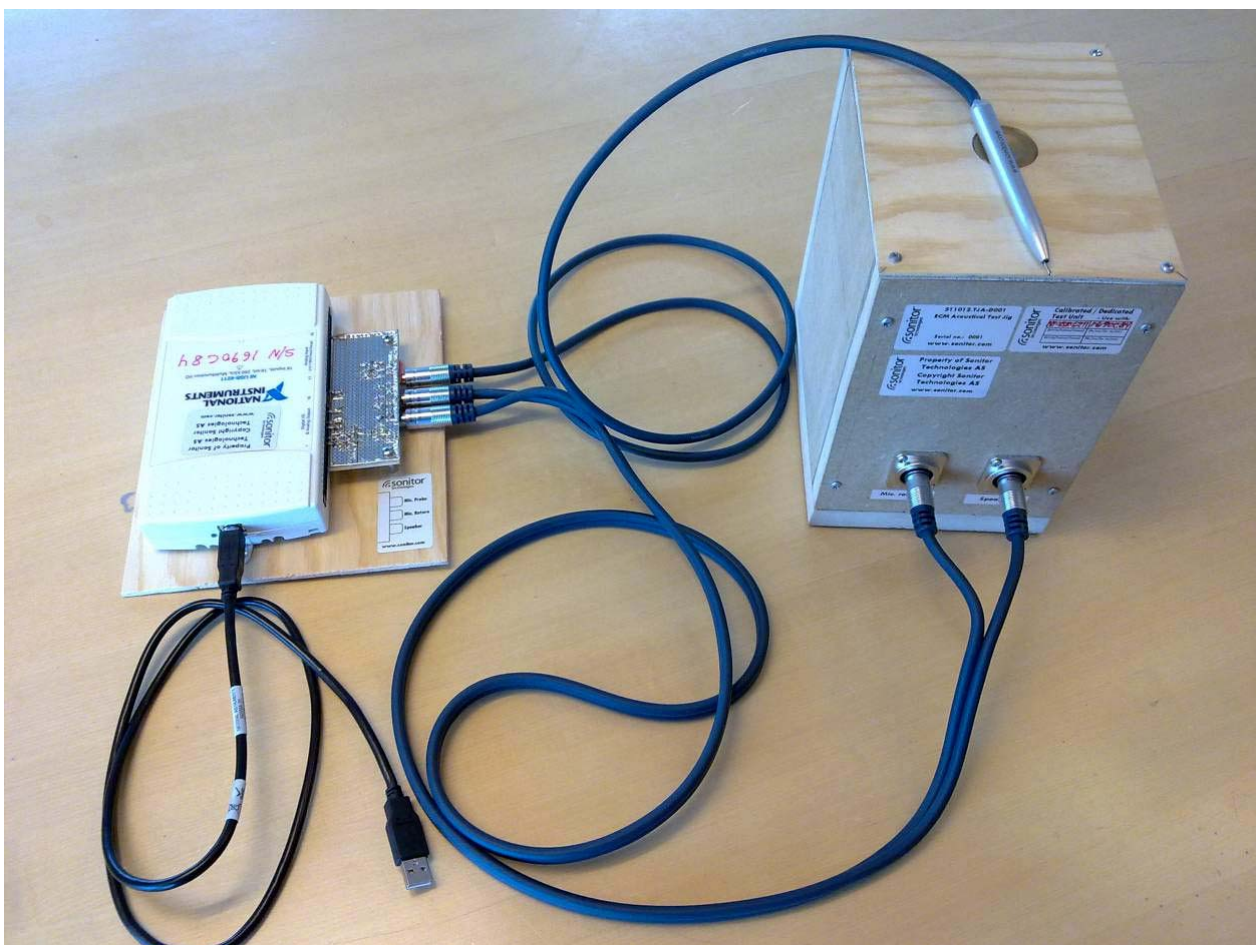


*Figure 17 ECM measurement setup developed as part of this project to achieve repeatable acoustic sensitivity measurements.*

Sonitor developed a Labview based measurement setup to implement the above method. It was found to be capable of delivering a repeatability of 1 dB in sensitivity measurements between 10-100 kHz. The sensitivity accuracy is of the order of 2 dB.

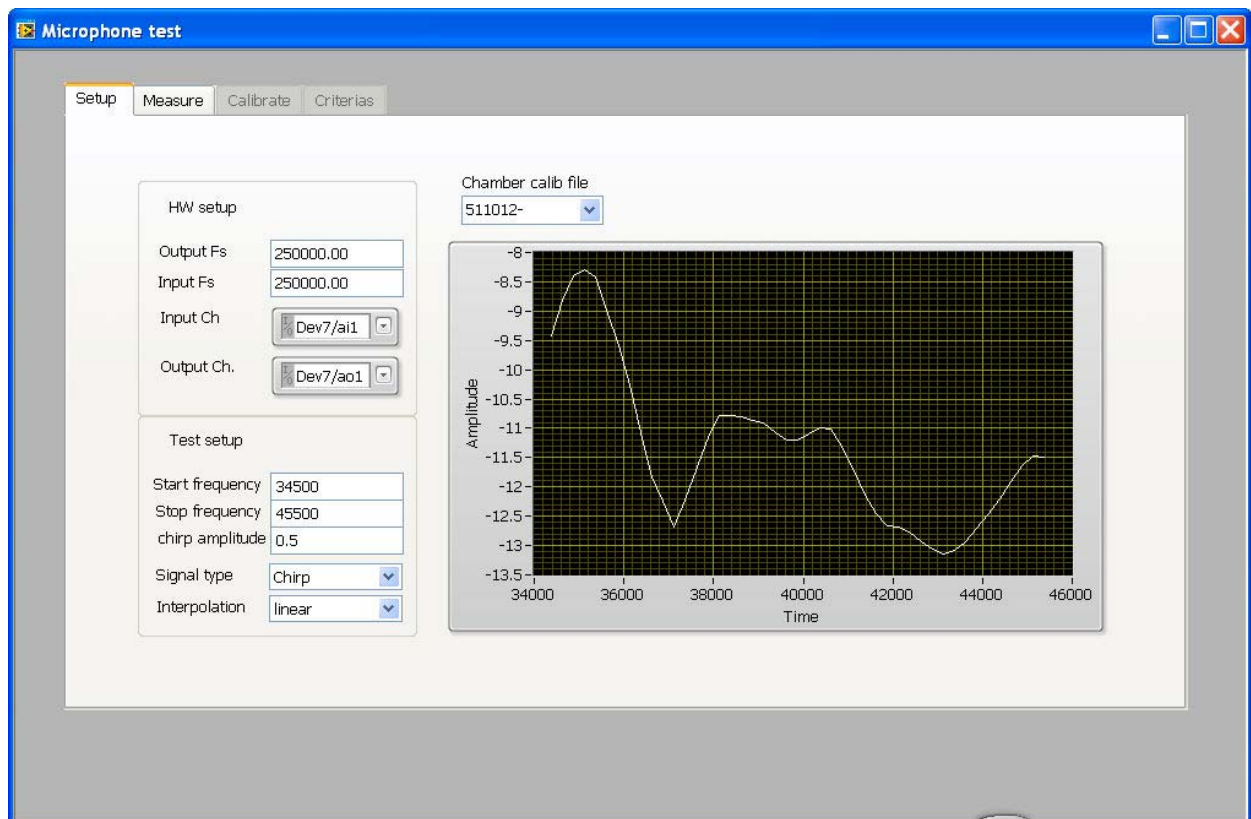


Figure 18 Calibration sensitivity trace measured using a B&K measurement microphone.



*Figure 19 Actual microphone sensitivity measurement on a ECM showing the result of compensating for the acoustic characteristics of the anechoic chamber.*

### **3.4.3 Sensitivity characterization of piezovolume devices**

The setup described earlier was adapted to characterize piezovolume devices. The following adaptation were made to compensate for the poor sensitivity of the piezovolume devices.

- The excitation voltage was increased to the maximum allowable voltage for driving the electret speaker (10V)
- The ADC gain was increased to 1000 to compensate for the low signal level encountered

Despite these efforts the performance of the setup was found to be wanting in repeatability, with a resulting repeatability of only 20 dB in the frequency range of interest. The result was partly due to the lacking ability to compensate fully for the reflection coming from the microphone mount. Mostly however it was due to the extremely low voltage levels resulting from the excitation signal available. Lack of time ultimately meant we had to abandon our goal of characterising element sensitivity repeatability with the help of this measurement setup.

## **3.5 Replacing ECM with piezoMEMS based microphones**

### **3.6 Background**

Since ECM's have been the dominant microphone solution for several decades now, virtually all consumer electronics devices that include audio functionality provide a ready interface for connecting ECM's. A typical example is the 3.5 mm jack found in many PC's and similar devices for connecting an external microphone. Such a ready ECM interface has the following characteristics:

- 2-3 V phantom power on the signal line supplying up to 300  $\mu$ A current to a JFET
- Capacitively coupled signal path to external high gain amplifier
- Ground

The ECM interface has such a dominant position that when MEMS microphones were introduced, the internal amplifier in these devices were designed to be compatible. Only recently a much more optimal interface for such devices is finding its way into the industry; the all digital PDM (Pulse Density Modulated) interface.

One important advantage of piezo-electric MEMS over more conventional technology such as capacitively sensing is the much reduced complexity of read-out electronics. Provided adequate sensitivity of the MEMS device, the readout can simply consist of a JFET acting as an impedance converter. This will provide a very large cost advantage over alternate MEMS solution.

One of the greatest challenges for PiezoMEMS based microphones will be stability of sensitivity over time. Since the current piezovolume devices were proving resistant to accurate sensitivity measurements, device stability was assessed through the use of impedance measurements under different poling conditions that might be viewed as accelerated aging experiments. One has to realise that even in consumer products, microphones might reach internal temperature of 65 degrees or more when the device is exposed to direct sunlight.

### 3.7 Impedance Measurement results

- 1 Poling procedure, 120 °C, 36V, 10 min
- 2 First poled with "positive" voltage, after measuring the electrical impedance over 1-1.5 h, the microphones were poled with opposite polarity.
- 3 The first measurement electrical impedance was taken as soon as possible after poling (3-4 min).

To assess stability of the resonance frequency we take once again a look at some results from D3.4.

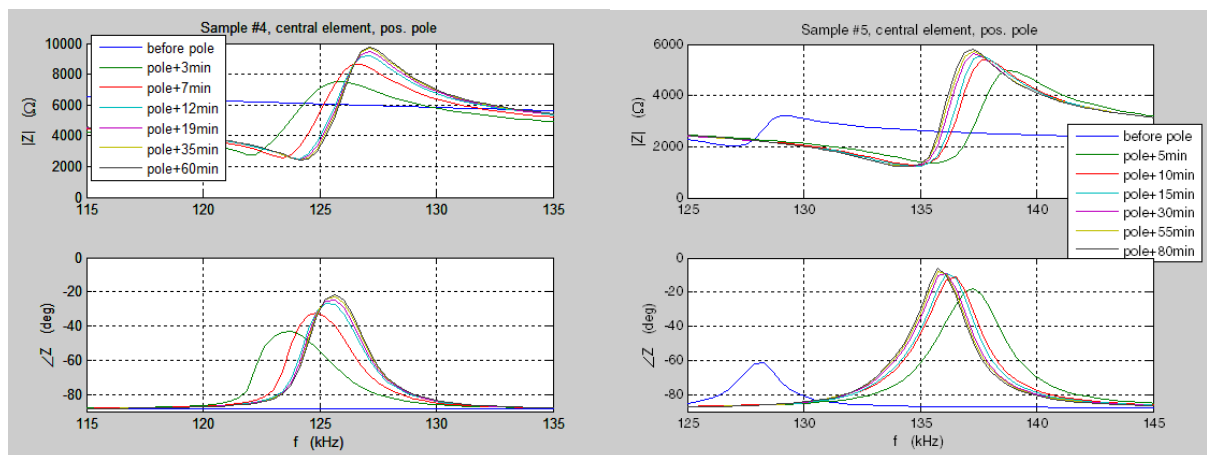


Figure 20 Impedance measurements d31 sample 3 and 5 GEN 1.

The very different behavior of two near identical devices when poled is of concern because it is a strong indication that these devices will drift in very different ways as they age.

### 3.8 Conclusions

- The piezo-volume microphone devices exhibited resonance features that are indicative of very high quality electro-mechanical coupling.
- The mechanical design limitations imposed by the multiple project wafer nature, imposes strong limitations on the sensitivity of the realized devices, limiting their sensitivity to -82 dB, at least 40 dB underperforming state of the art high volume microphones.
- Device sensitivity was too low to be able to use more conventional microphone characterisation approaches adapted from ECM characterization.
- Fatigue effects do not play a significant role in piezoMEMS based microphones due to the extremely low forces exerted by the acoustic excitation.
- Long term sensitivity of PiezoMEMS devices is of concern given the low temperature required to depole these devices.

## 4 VERMON PMUT

Figure 21 gives a layout of Vermon's pMUT design. This design was aimed at producing a high power transducer operating around 1 MHz in water. The active transducing area was set at 6 mm diameter. Using the membrane characteristics set by the process this led to membranes around 120  $\mu\text{m}$  in diameter (three subtypes were designed with 110, 120 and 130  $\mu\text{m}$ ). Due to the limitations of the production process, membranes had to be spaced from each other by 300  $\mu\text{m}$ . The consequence of that limitation is a low active surface ratio (10,7%, 12,8%, or 15% depending of the chosen membrane size). For comparison, cMUT transducers manufactured with surface micromachining process have an active surface ratio (ratio of membranes surface over total area) of roughly 70%.

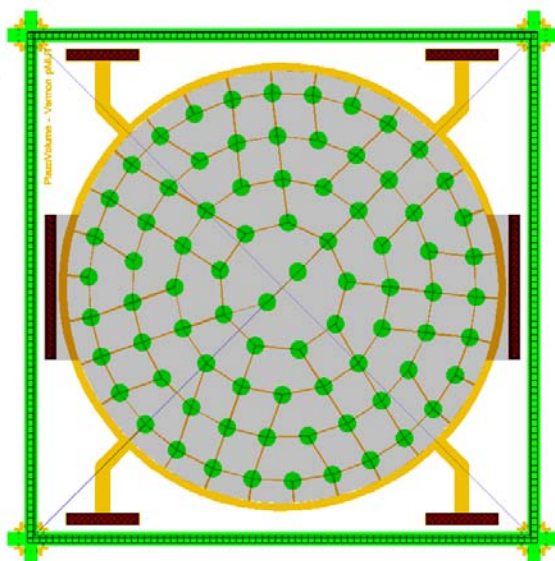


Figure 21 pMUT layout

In this document, the transduction capacity of those elements was evaluated.

### 4.1 Geometric control

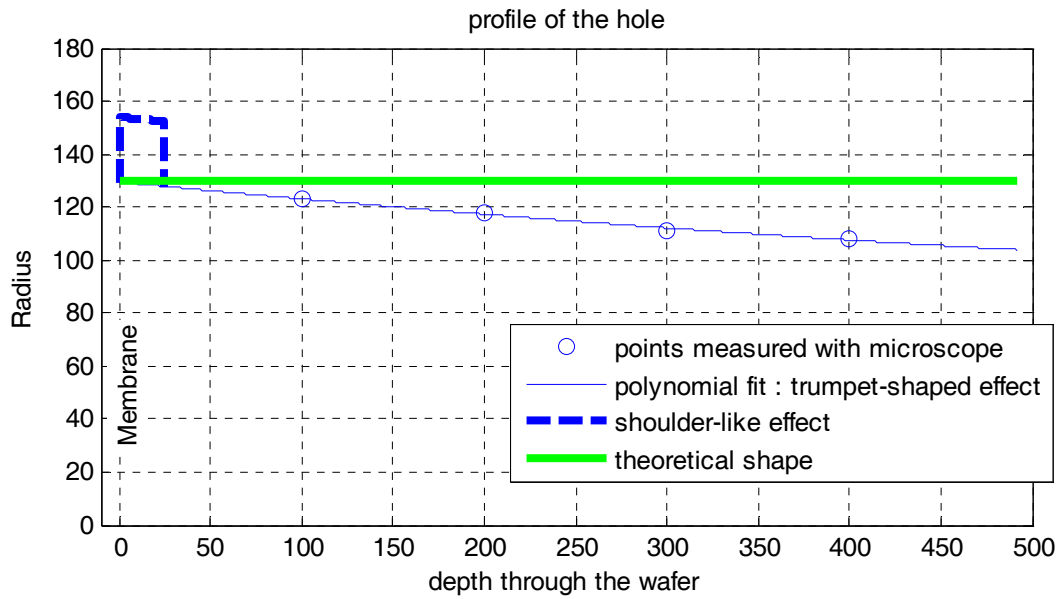
The size of the membrane is influenced by imperfection in the DRIE etching.

The figures below give the profile of the DRIE drilling for each of the three membranes. The top side of the wafer (membrane) is on the left of each plot. The green line gives the theoretical perfect shape (cylinder of 130  $\mu\text{m}$  radius). The blue line is the trumpet shaped profile

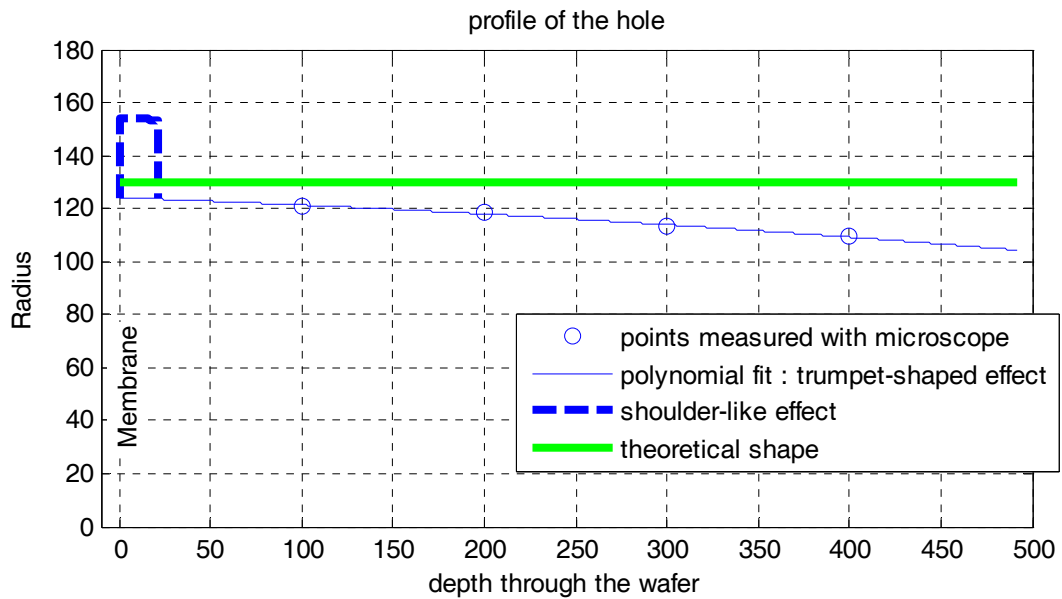
Overall, the membranes are about 30  $\mu\text{m}$  larger (diameter) than design. Using clamped circular plate formula, a radius of 160  $\mu\text{m}$  instead of 130 lowers the resonance frequency (for every mode) by 33%. It also changes the relative amplitude the modes: the electrode is no longer placed optimally to excite selectively the fundamental mode.

The same kind of measurement was done on phase I samples, and the results are very similar.

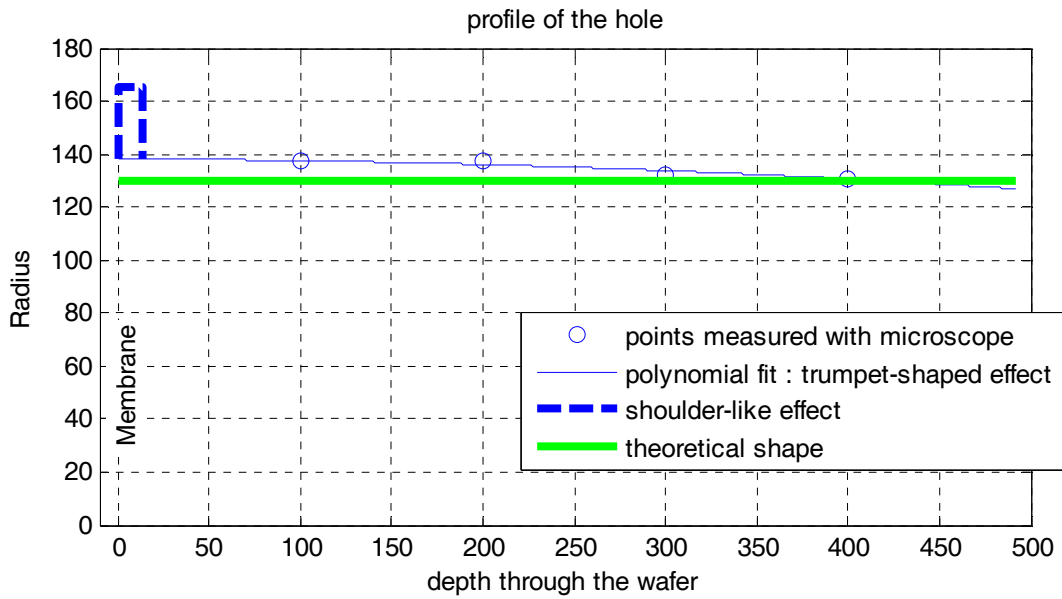
Membrane 1 :



Membrane 2 :



Membrane 3



## 4.2 Identification of modes by impedance measurements in air

### 4.2.1 Modes of a clamped circular membrane

Vibration modes are designated with two indexes, m and n, which are the mode counts along  $\varphi$  and r axis respectively. The figure below displays the shape of the first 12 modes : the black lines are the nodes (lines along which displacement is zero).

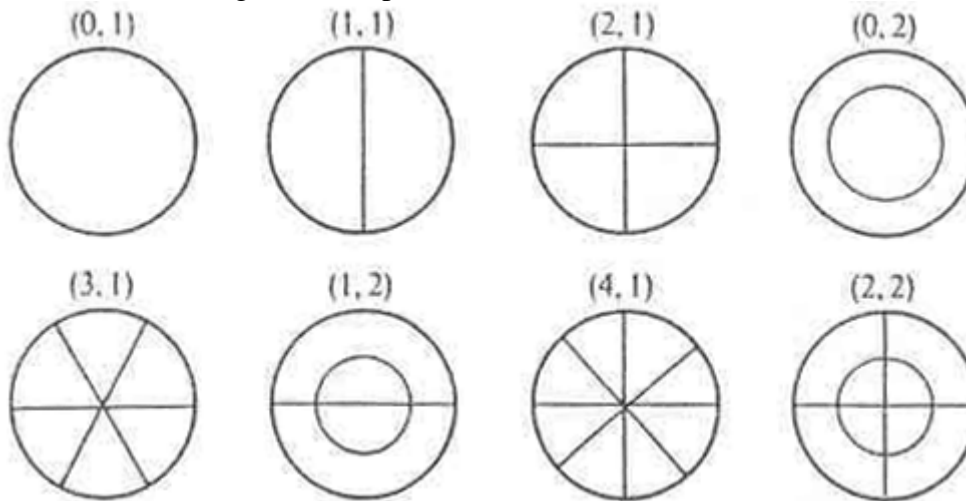


Figure 22 Modes of a clamped circular membrane

$f_{01}$  is the frequency of the fundamental mode (function of thickness, diameter and material's Young's Modulus and Poisson ratio), the frequency of higher modes is given proportionally to it.

$$f_{11} = 2.06f_{01}, f_{21} = 3.41f_{01}, f_{02} = 3.89f_{01}, f_{31} = 5.00f_{01}, f_{41} = 6.62f_{01}$$

### 4.2.2 Impedance measurement

The impedance of a sample of each sub-design (B1 to C3) was electrically characterized using a 4294A impedance analyzer. For the measurements, a DC bias of 10 volts forward is applied. The impedance measurement emphasizes the various resonance modes. The most strongly coupled mode seems to be the (0,2).

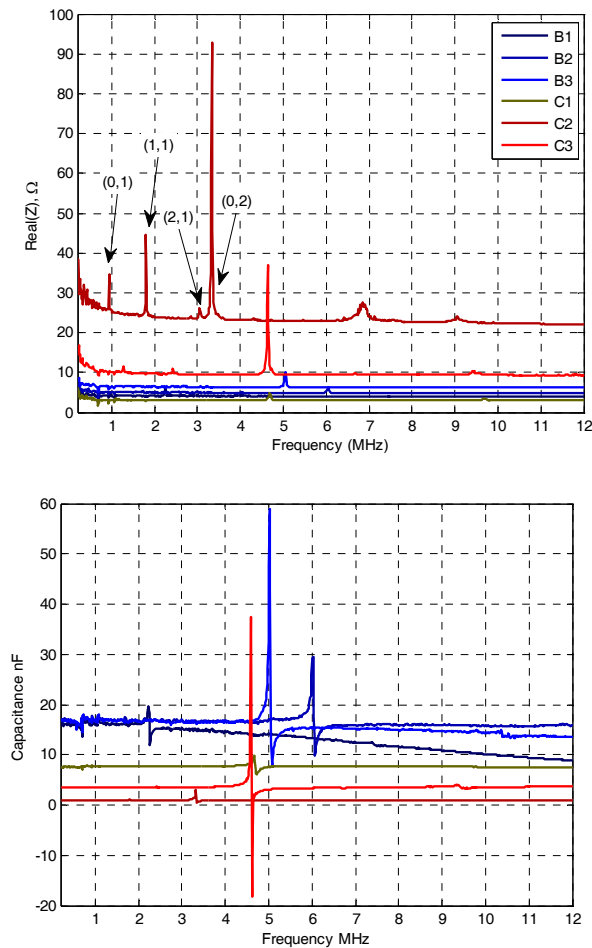
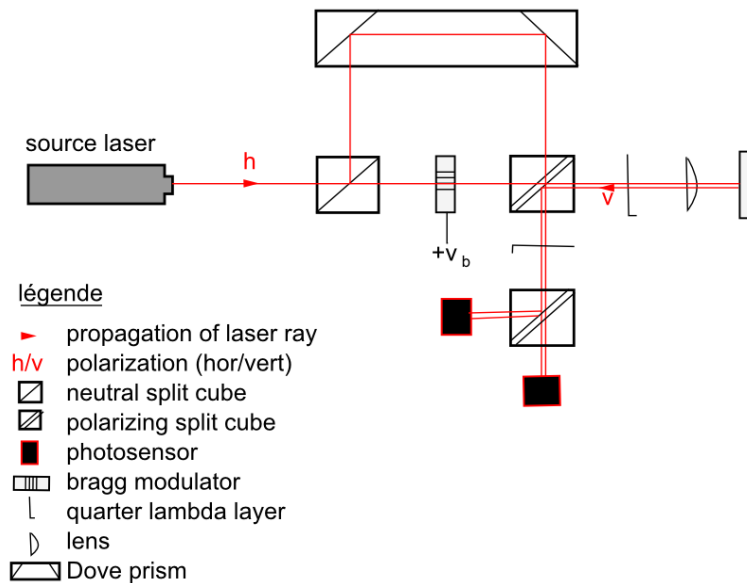


Figure 23 : Modes of a clamped circular membrane

## 4.3 Laser interferometry measurements

### 4.3.1 Principle



Heterodyne laser interferometers use a modulation on the probe signal. In the equipment used here, the frequency of this modulation is 140 MHz. The measured sample has to be reflective. After analogic demodulation, a radiofrequency electric signal is obtained, which is directly proportional to the displacement of the measured surface. In the results given in this document, the displacement value is given.

For all measurements hereafter, a DC bias of ten volts forward is applied on the pMUT.

The sample used for those tests is a C1 type. As the membranes are significantly larger than design due to DRIE geometry, the smaller type was selected to reduce the frequency shift.

### 4.3.2 Measurements in air

A single 2.5 Mhz sinusoidal pulse is applied. This wideband excitation reveals all the resonance modes of the membrane.

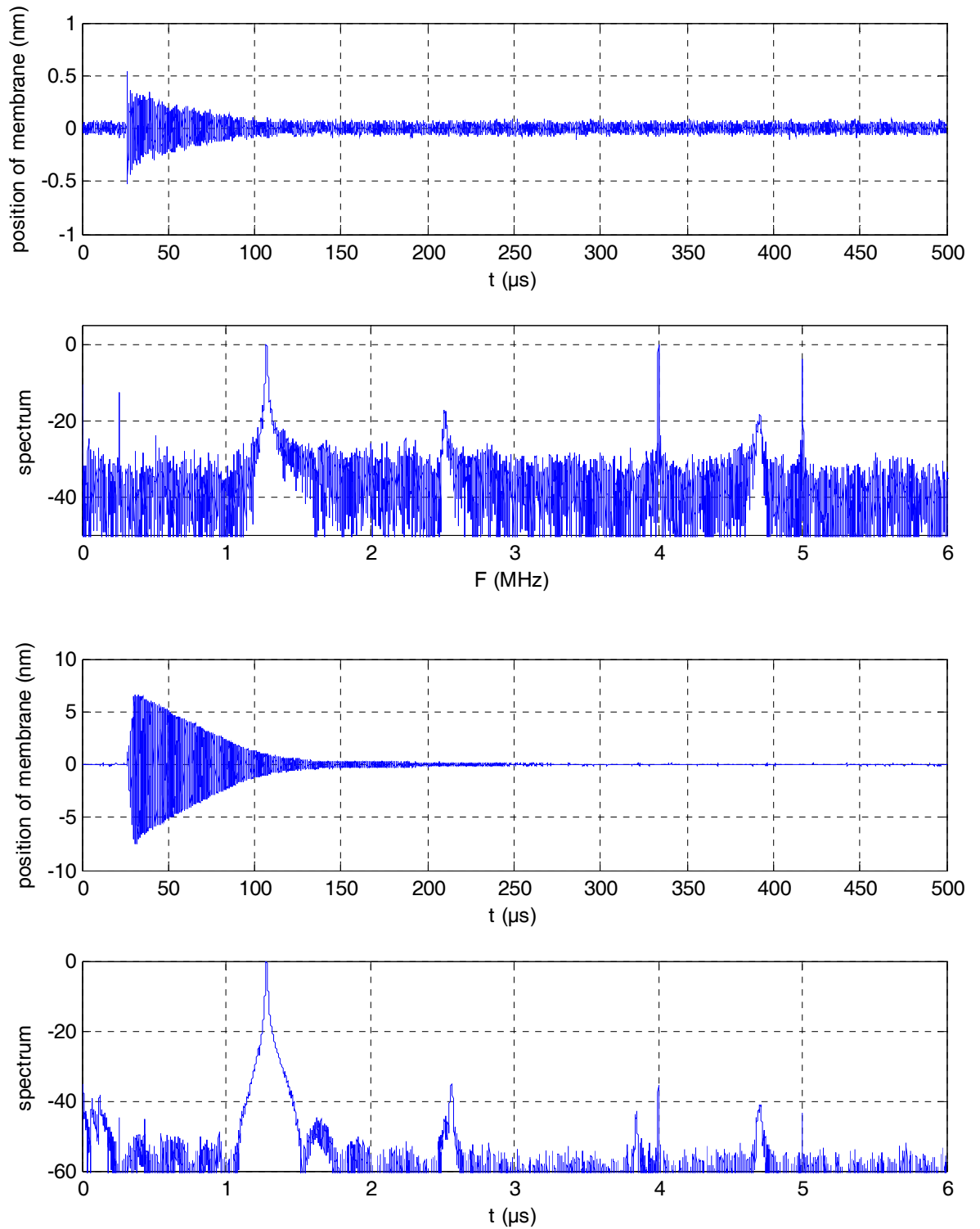


Figure 24 Results in air for a single 2.5 MHz pulse of amplitude 1 Vpp (top) or 10 Vpp (bottom)

### 4.3.3 Measurements in oil

The displacement in air provide a proof of the functionality of a transducer (existence of electro-acoustic coupling) but not of the performances. The transducer developed in this project being initially intended for HIFU applications, the main indicator of its performance is the amplitude of the acoustic wave that can be generated.

For fluid coupling evaluation, the sample was immersed in oil. Oil provides acoustic properties similar to water, while also ensuring electrical insulation.

The measurements performed in oil are divided by a factor of 1.47 (optical refraction index) to obtain displacement values.

### 4.3.4 Wideband excitation

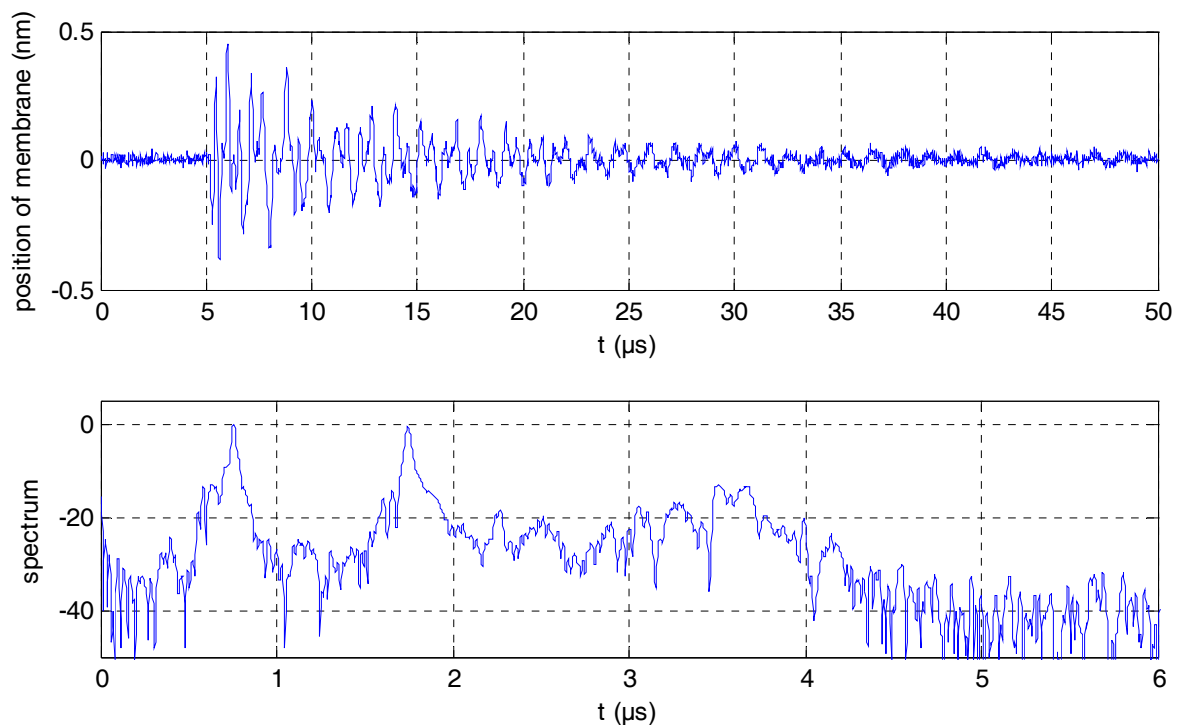


Figure 25 Results in oil for a single 2.5 MHz pulse of amplitude 1 Vpp (top) or 10 Vpp (bottom)

The same excitation is used, that was previously applied in air. The impact of fluid damped (radiation of energy into surrounding oil) is obvious. Resonance amplitude is lowered by an order of magnitude, while the main mode frequency is reduced from 1.3 to 0.75 MHz.

This is lower than design as the target was 1 MHz. This difference is explained by the larger diameter of the membrane.

#### 4.3.5 Narrow band excitation at 750 kHz

Still with fluid coupling, the device is excited with a continuous wave at 750 kHz (main mode frequency in fluid coupling). Then the excitation amplitude was gradually increased to 40 Volts, which earlier measurements had shown was an approximate maximal amplitude that could be applied without damaging the samples.

The measurement at 40 Vpp excitation is used as a reference in the next section to estimate the maximal transducer power.

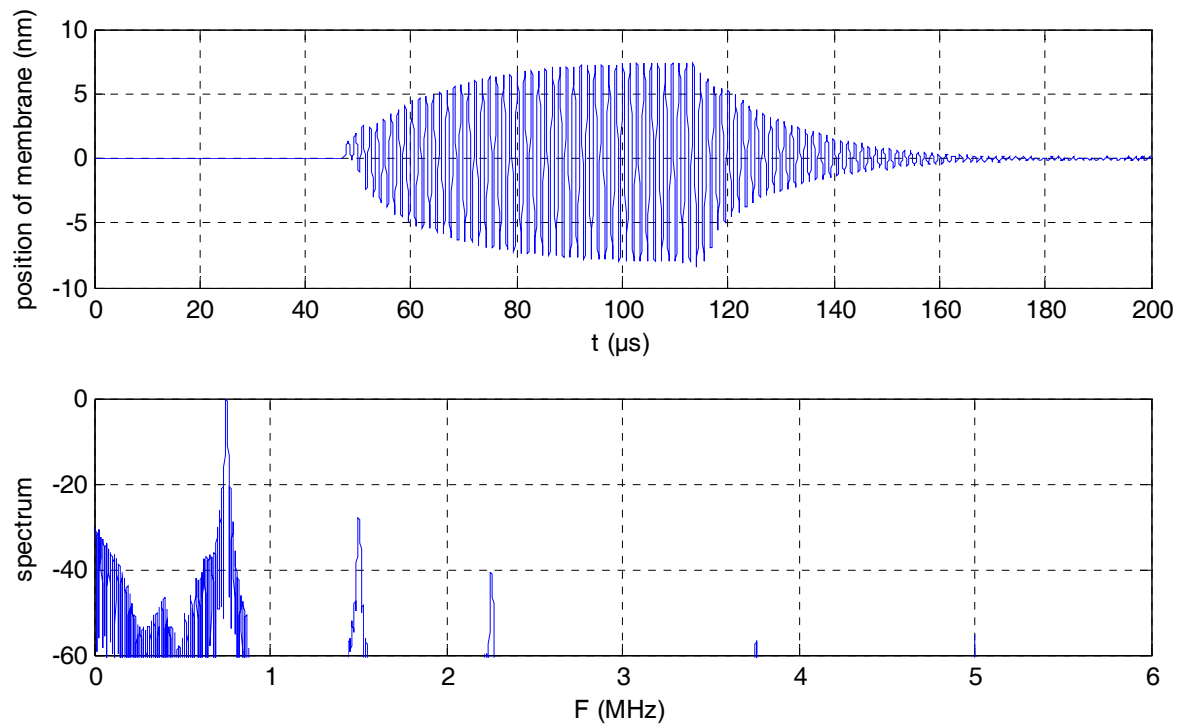


*Figure 26 750 kHz, 20 Vpp, 50 cycles excitation in oil*

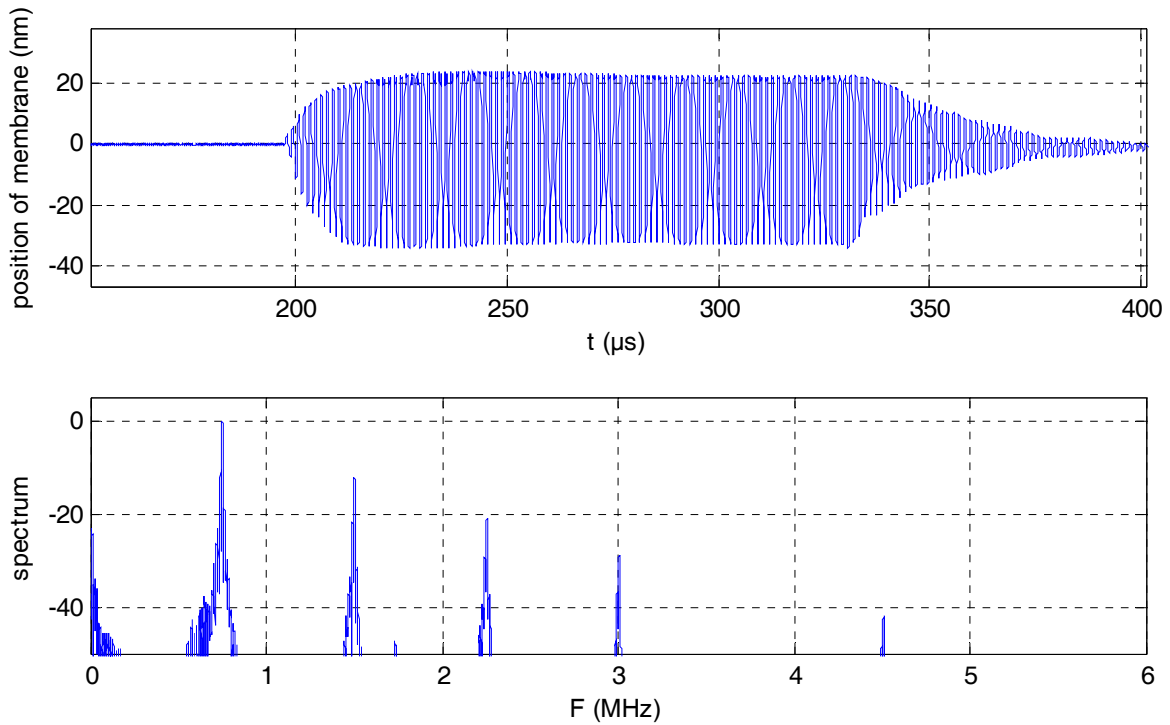


Figure 27 750 kHz, 40 Vpp, 100 cycles excitation in oil

#### 4.3.6 Conversion to acoustic intensity

As the dimensions of the individual membranes are very small compared to the wavelength, we can assimilate each one as a point source.

A power transducer is evaluated by the acoustic intensity, which is the measure of the acoustic power per surface unit. It is usually measured on the surface of the transducer, which gives a value independent of focalisation.

For a plane harmonic wave, acoustic intensity is defined as follow :

$$I = \frac{P_{max}}{2Z} = \frac{Z \cdot V_{max}^2}{2} = \frac{Z \cdot \omega^2 \cdot X_{max}^2}{2}$$

Where Z is the acoustic impedance of the medium (in rayleigh or kg.s/m<sup>2</sup>), and  $P_{max}$ ,  $V_{max}$ ,  $u_{max}$  are the peak values of acoustic pressure, particular speed and displacement respectively.

$$u_{max,transducer} = F_{fitting} \times F_{mode} \times u_{max,membrane\ center}$$

Where  $F_{mode}$  is the ratio between the average displacement of the whole membrane and the displacement of the center point, which for the fundamental mode of a clamped circular membrane can be well approximated as 1/3.  $F_{fitting}$  is the fraction of the transducer area which is covered with membranes.

Using the 50 nm amplitude obtained for 40 V<sub>pp</sub> excitation, this formula results in only **1.2 mW/cm<sup>2</sup>**, for a peak pressure of 6 kPa. This value is extremely low, as HIFU transducers are expected to produce several watts per cm<sup>2</sup>. The pressure of 6 kPa is barely enough for an hydrophone measurement.

#### 4.4 Conclusion

Several positive aspects appear when evaluating those devices :

- Integration on PCBs have been successful
- Phase II devices as received were all functional
- Large displacements were obtained on the membranes.
- 

However, the devices failed to prove the suitability of the technology for HIFU applications, because once converted to displacement on the full transducer area, the acoustic power delivered by the devices is actually extremely small, missing three orders of magnitude (60 dB) compared to regular HIFU devices.

Part on the gap could in theory be compensated by increasing the very low surface coverage ratio.

On the positive aspect, taking into account the intrinsic impedance of PMUT devices, there is high expectation for **matrix array transducers** for 3D imaging applications where each transducer is very small surface area and the dielectric behaviour of PMUT will help to design efficient apparatus, this will be done as further actions after the project. Vermon will perform a new matrix design for PMUT and will work with the consortium to promote this technology.